Surface Review and Letters, Vol. 24, No. 8 (2017) 1750110 (12 pages)

DOI: 10.1142/S0218625X17501104

STUDYING STRUCTURAL, OPTICAL, ELECTRICAL, AND SENSING PROPERTIES OF NANOCRYSTALLINE SnO_2:Cu FILMS PREPARED BY SOL–GEL METHOD FOR CO GAS SENSOR APPLICATION AT LOW TEMPERATURE

SELMA M. H. AL-JAWAD*,‡, ABDULHUSSAIN K. ELTTAYF† and AMEL S. SABER†

*School of Applied Sciences, University of Technology, Baghdad, Iraq

†Ministry of Science and Technology, Iraq

‡Salma_aljawad@yahoo.com

Received 8 August 2016
Revised 23 December 2016
Accepted 14 February 2017
Published 28 March 2017

Nanocrystalline SnO_2 and SnO_2:Cu thin films derived from $SnCl_2 \cdot 2H_2O$ precursors have been prepared on glass substrates using sol–gel dip-coating technique. The deposited film was 300 ± 20 nm thick and the films were annealed in air at 500°C for 1 h. Structural, optical and sensing properties of the films were studied under different preparation conditions, such as Cu-doping concentration of 2%, 4% and 6 wt.%. X-ray diffraction studies show the polycrystalline nature with tetragonal rutile structure of SnO_2 and Cu:SnO_2 thin films. The films have highly preferred orientation along (110). The crystallite size of the prepared samples reduced with increasing Cu-doping concentrations and the addition of Cu as dopants changed the structural properties of the thin films. Surface morphology was determined through scanning electron microscopy and atomic force microscopy. Results show that the particle size decreased as doping concentration increased. The films have moderate optical transmission (up to 82.4% at 800 nm), and the transmittance, absorption coefficient and energy gap at different Cu-doping concentration were measured and calculated. Results show that Cu-doping decreased the transmittance and energy gap whereas it increased the absorption coefficient. Two peaks were noted with Cu-doping concentration of 0–6 wt.%; the first peak was positioned exactly at 320 nm ultraviolet emission and the second was positioned at 430–480 nm. Moreover, emission bands were noticed in the photoluminescence spectra of Cu:SnO_2. The electrical properties of SnO_2 films include DC electrical conductivity, showing that the films have two activation energies, namely, E_{a1} and E_{a2}, which increase as Cu-doping concentration increases. Cudoped nanocrystalline SnO_2 gas-sensing material has better sensitivity to CO gas compared with pure SnO_2.

Keywords: SnO_2; structure properties; optical properties; sol–gel; scanning electron microscopy; Cu-doping; activation energy.

1. Introduction

Metal oxide semiconductors, such as SnO_2, ZnO, In_2O_3 and Nb_2O_5, are widely used for detecting toxic gases, including NH_3, H_2, and CO. Tin oxide (SnO_2), an n-type semiconductor, has a tetragonal rutile structure with lattice parameter of $a = b = 4.737$ Å and $c = 3.187$ Å and a direct optical band gap of approximately 3.6 eV. SnO_2 has attracted considerable

attention because of its low cost and high sensitivity.[1–5] The addition of metal ions as impurities likely plays an important role in varying the charge carrier concentricity of the metal oxide matrix, catalytic material activity, surface potential, and crystallite size.[6] Cu,[7] Fe,[6] Ag,[8] Mn,[9] Pt,[10] and Nd[11] are doped to improve the SnO_2 characteristics. Doping with Cu results in better sensitivity and selectivity of SnO_2 towards CO gas compared with that of pure SnO_2. Mishjil *et al.* reported that Cu addition stabilizes the SnO_2 surface and increasing Cu content decreases SnO_2 grain size.[7] Williams *et al.* presented the use of SnO_2 thin film for sensing CO from a car exhaust and found the sensor to operate at 125°C.[12] Parthibavarman *et al.* reported that the addition of Cu at 10 and 20 wt.% decreased the structural and optical properties, specifically, the grain size and optical band energy of SnO_2 nanopowders prepared through chemical precipitation.[13] Several methods, such as electrostatic spray deposition,[6,14] laser chemical vapor deposition,[15] solvothermal,[16] and sol–gel,[17] are used to produce SnO_2 or doped SnO_2 thin films. Among these techniques, the dip-coating method is attractive because of its simplicity, capability to produce good-quality films at a large scale, safe operation, low cost of equipment, and easy handling of chemical components.[18–20] This work aims to develop a sensor that has superior characteristics, i.e. higher sensitivity at room temperature, for CO detection.

2. Experimental

2.1. *Materials*

The primary precursors for synthesis of SnO_2 include $SnCl_2 \cdot 2H_2O$ (chloride dehydrate 96%; Fisons, England), $CuCl_2 \cdot 2H_2O$, C_2H_5OH (ethanol 99%; Scharlau, Spain), and $C_3H_8O_3$ glycerin. These chemicals were used without further purifications.

2.2. *Preparation of solution*

A total of 2 g $SnCl_2 \cdot H_2O$ was dissolved in 15 mL ethanol for Cu-doping. $CuCl_2$ was added to the starting solution, in which the volumetric ratios of Cu were 2, 4, and 6 wt.%. The solution was stirred for 1 h with a magnetic stirring apparatus at a temperature of 75–80°C. Then, solution (sol) was mixed with glycerin as a dissipation stabilizer to obtain the sol–gel through dip-coating.

2.3. *Deposition of the films*

Films from the sol are preferred for use in dip-coating technique. The substrates ($26 \times 76 \times 1$ mm glass slides) were cleaned by emerging in ultrasonic bath for 5 min and then rinsing with ethanol. Thus, given that all substrates were dipped into the sol, they were slowly withdrawn from the bath at a fixed speed of 80 mm/min. All films were first dried at 100°C for 30 min and then subjected to heat treatment at 500°C for 1 h.

The crystal structure of SnO_2 films was analyzed using X-ray diffraction (XRD, Shimadzu) with CuKα1 radiation at $\lambda = 1.54$ Å. The crystallite size was calculated using Scherer equation[15]:

$$D = k\lambda/\beta \cos\theta, \tag{1}$$

where k is constant as 0. 9, λ is the X-ray wavelength of 1.54 Å, β is the full width at half maximum (FWHM) and θ is the Bragg diffraction angle of the XRD peak (degree). The morphologies of the resulting films were characterized through atomic force microscopy (AFM) (CSPM-5000) and scanning electron microscopy (SEM) (VEGA TE SCAN). The optical transmittance and absorbance were measured using UV/VIS spectrophotometer (UV-1800 Shimadzu) with double beam in wavelength range of 300–1000 nm. Photoluminescence (PL) has been measured using a fluorescence spectrophotometer (CARY Eclipse).

Aluminum sheets were used to achieve the desired electrode shape. To provide electrical properties, the masks were prepared from aluminum foil. These masks have similar dimensions to that of the substrate and after they were cleaned, the masks were attached and fixed to cover the substrate. These masks are attached on films to depose the aluminum on the SnO_2 film surface using vacuum thermal evaporation technique. Tangiesten (W) boat material under 10^{-5} Torr pressure is used for electrical and sensing measurement, with aluminum pole width at 2 mm.

The electrical resistivity of SnO_2 films is an important parameter for its applications. Electrical sensitivity can be calculated from the change in thin film resistance with temperature and can be used to study the variation of film sheet resistance in different temperatures. In this study, the electrical resistivity of SnO_2 films was evaluated by putting the film in a thermal oven (Griffin Incubator). A digital

electrometer is used to measure the variation in film resistance with different temperatures. Electrical sensitivity has been measured from thermocouple wire and film resistance for every 10°C was recorded, starting from room temperature until 150°C.

Hall effect measurements using a HMS 3000 (EcopiA) were used to establish the charge carrier type and carrier concentration of the semiconductor.

3. Results and Discussion

3.1. *XRD analysis*

The XRD patterns for thin films of Cu-doped SnO_2 in various Cu-doping levels, namely 0, 2, 4, and 6 wt.%, are shown in Fig. 1. All films are polycrystalline, with rutile-phase SnO_2 crystallites with tetragonal structure and the peak positions of the films were found to be in good agreement with the established standards (JCPDS No. 41-1445). In (110), (101), (200), (211), and (220) oriented growth, no peaks corresponding to Cu or CuO phase were noted, indicating that Cu has been successfully incorporated into tin sites in the SnO_2 lattice. This can be attributed to the

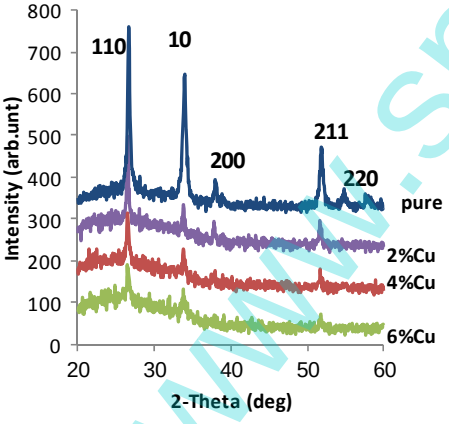

Fig. 1. (Color online) XRD pattern of SnO_2 thin films for different doping concentration of Cu.

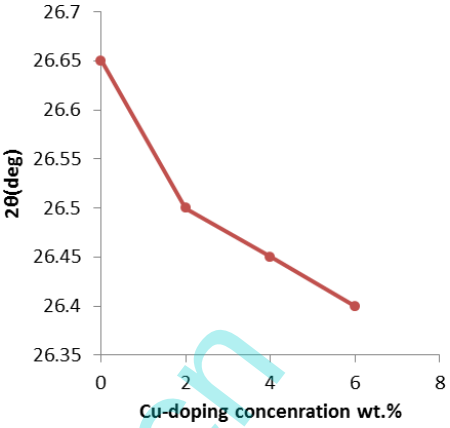

Fig. 2. (Color online) 2θ as a function of different doping concentrations of Cu for SnO_2 thin films.

substitution of Sn^{4+} ions with Cu^{2+} ion based on the comparable radii of Sn^{4+} and Cu^{2+} (0.69 and 0.74 Å).[19] The oxygen-ion vacancies resulting from substitutional doping of Sn^{4+} with Cu^{2+} are charged, compensated by electron-holes. Such vacancies reduced the 2Θ of values, which were 26.65°, 26.50°, 26.45°, and 26.40°, corresponding to the (110) plane peak with Cu concentrations of 0, 2, 4, and 6 wt.%, respectively. The lattice parameters (a and c) and unit cell volume reduced upon Cu-doping, as shown in Table 1 and Fig. 3. This result is in good agreement with Ref. 13. The FWHM of the diffraction peaks increases with increasing Cu concentration in the film, as illustrated in Fig. 4. Increase in FWHM along with reduction in peak intensity indicates that Cu is incorporated in SnO_2 lattice in thin films. The addition of Cu^{+2} significantly influenced the crystallinity of SnO_2, suggesting that the crystallinity of the thin films of Cu-doped SnO_2 may decrease compared with that of pure SnO_2 thin films. This may be caused by the formation of the stresses resulting from the varying ion sizes between Sn- and Cu-doped films. The sizes of the SnO_2 crystallite, which was

Table 1. XRD Measurements of SnO_2 thin films for different doping concentrations of Cu by Sol–gel (dip-coating).

Doping consecration of Cu	d Standard (110)	d Calculated (110)	a (Å)	c (Å)	Crystallite size (nm)	FWHM
Pure	3.347	3.3470	4.763	3.2	22	0.3654
2%	3.347	3.35635	4.75	3.19	17	0.4586
4%	3.347	3.34663	4.729	3.191	16	0.51030
6%	3.347	3.3469	4.73	3.186	12	0.6338

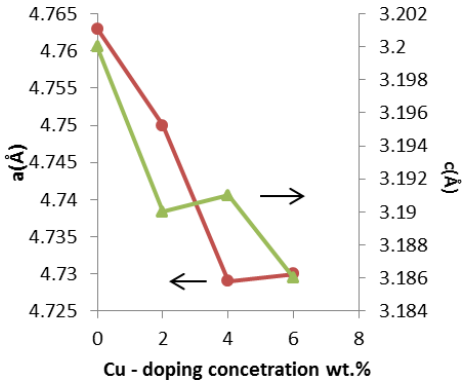

Fig. 3. (Color online) The Lattice constants (a&c) for SnO_2 thin films as a function to Cu-doping concentrations.

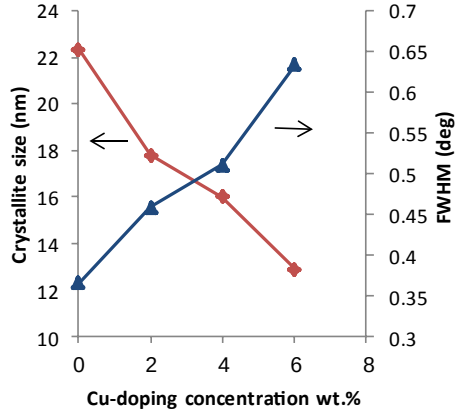

Fig. 4. (Color online) The main grain size and FWHM for SnO_2 thin film with Cu-doping concentrations.

calculated to be 22, 17, 16, and 12 nm using Scherrer formula, correspond to the peak of (110) plane, with a Cu-doping in solution of 0, 2, 4, and 6 wt.% respectively. This result is in good agreement with Refs. 7,11 and 21. Figure 4 displays the influence of Cu-doping concentration on the average crystallite size of the prepared SnO_2 thin films. As shown, increased Cu concentration decreases the average crystallite size. The different doping concentrations of Cu, which was measured through XRD, in SnO_2 thin films, are illustrated in Table 1.

3.2. *Morphological analysis*

Figure 5 reveals the 2D and 3D AFM images of pure SnO_2 thin films doped with 4 and 6 wt.% Cu concentrations. The average grain size, which is measured from AFM analysis using software, of doped and nondoped synthesized SnO_2 films ranged from 91 nm to 75 nm. AFM results show that adding Cu to SnO_2 thin films causes the films to become rough and porous and have a small grain size. This result is in good agreement with Ref. 22. Table 2 shows the grain size, roughness values, and root mean square of SnO_2 thin films.

Figure 6 shows the SEM images displaying the surface morphology of the pure and Cu-doped SnO_2 films on glass substrate. The SEM images clearly

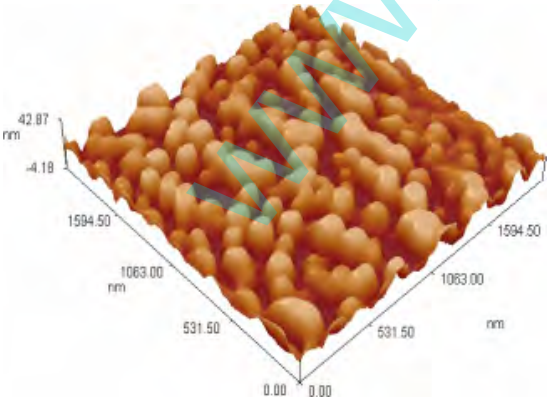

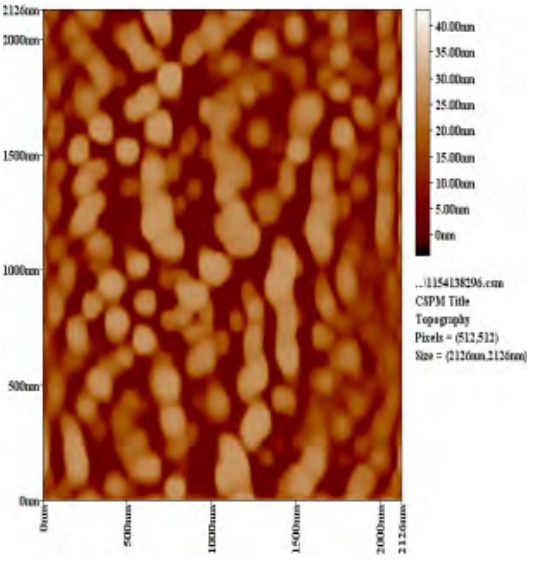

(a)

Fig. 5. 2D and 3D AFM images of SnO_2 thin films at various doping concentrations (a) pure (b) 4% Cu and (c) 6% Cu.

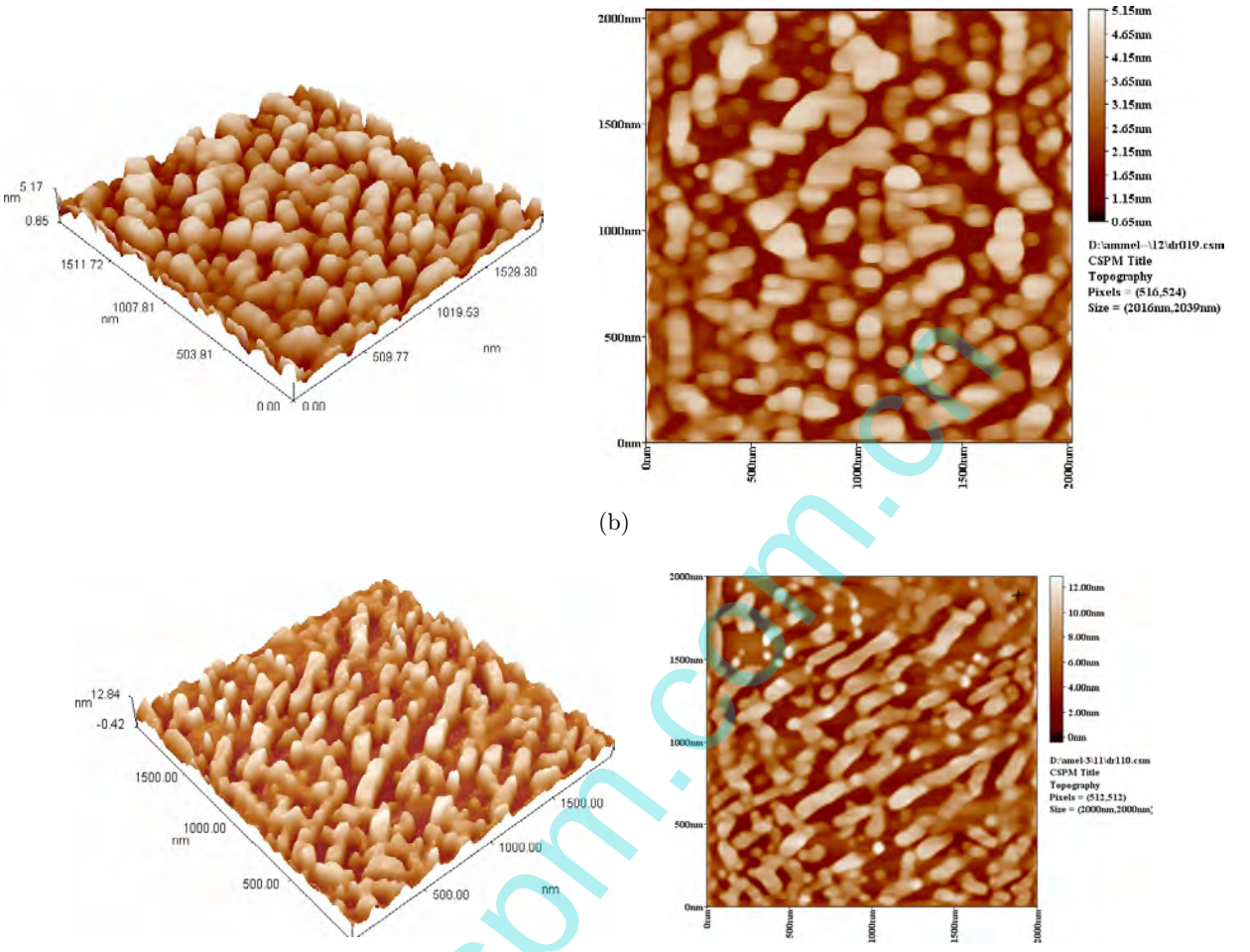

Fig. 5. (*Continued*)

illustrate the formation of spherical particle. Furthermore, both pure and doped films have a homogeneous surface morphology, are dense with low porosity and adhere well to the substrate without any cracks. The grain sizes measured from the SEM images are 79, 71, and 61 nm at 0, 4, and 6 wt.% Cu, respectively. The particles were uniformly distributed in these films, with a decrease in average particle size as the Cu-doping concentration increased. Cu-doping in the SnO_2 films also altered the shape of these particles. Small-sized particles were uniformly distributed in the nondoped film, which has

Table 2. Grain size and root mean square of surface roughness obtained from AFM data.

Cu-concentration	Grain size (nm) AFM	Roughness (nm)	RMS (nm)
Pure	91	1	1.1
4%	85	2	2.4
6%	75	3	3.7

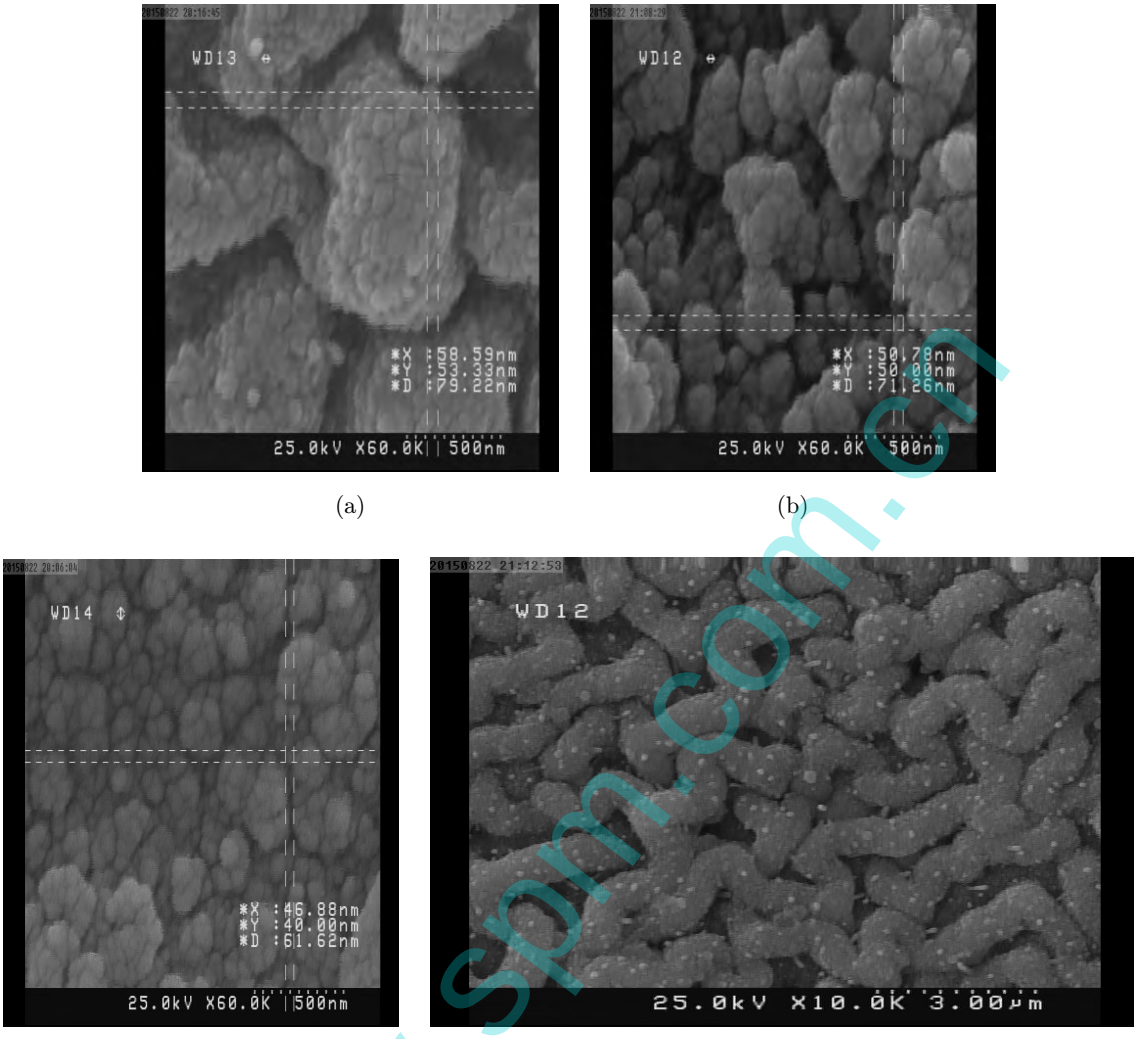

Fig. 6. (Color online) The SEM image (top view) of SnO_2 thin films (a) pure (b) 4% Cu (c) 6 wt.% Cu, (d) 6 wt.% Cu with low magnification.

agglomerated particles compared with the doped films. This further confirms the increase in stacking fault density and these results are in agreement with the previous XRD results. The low-magnification SEM image of films at 6 wt.% Cu-doping is shown in Fig. 6(d). The influence of Cu on the surface morphology of the thin films is evident through the appearance of small, white grains shaped like the large intestine. These results are in agreement with that of previous studies.[13] This kind of outgrowth assists the application of these films as a gas sensor because the film has a wide open surface to be exposed to the gas. The average grain size, which was obtained using Scherrer–Debye formula, is smaller than that estimated from AFM and SEM measurements, indicating that grains are probably an aggregate of many crystallites.

4. Optical Studies

Figure 7 shows the optical transmittance spectrum of Cu-doped SnO_2 films at various doping concentrations. The transmittance of the deposited films was measured under ultraviolet (UV)–Vis regions of the electromagnetic spectrum. The transmittance of the films decreased from 82.4% to 65.3% when the doping concentration increased from 0 wt.% to 6 wt.%. The optical transmittance values decreased with increase

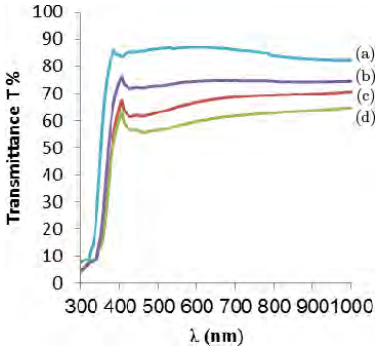

Fig. 7. (Color online) Variation of transmittance with wavelength of SnO_2 thin films for different doping concentrations of Cu ((a) pure, (b) 2% (c) 4%, (d) 6 wt.%) by Sol–gel (dip-coating).

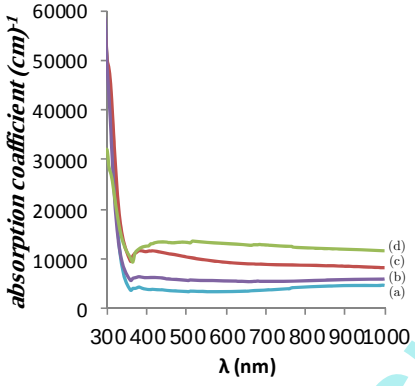

Fig. 8. (Color online) Variation of absorption coefficient α with wavelength of SnO_2 thin films for different doping concentrations of Cu ((a) pure, (b) 2% (c) 4%, (d) 6 wt.%) by Sol–gel (dip-coating).

in Cu concentration and this behavior is caused by the increase in set free electron as a result of the increase in Cu concentration. These results are in agreement with those of previous works.[7,11]

The absorption coefficient α was calculated using the following equation[8]:

$$\alpha = 2.303\, A/t, \tag{2}$$

where α is the absorption coefficient, A is the absorbance, and t is the film thickness. Figure 8 shows the change in the absorption coefficient of pure and doped films with varying wavelength. In general, the absorption coefficient decreases with the increase in wavelength. Moreover, the absorption coefficient also increases to greater than $10^4\,\mathrm{cm}^{-1}$ as the Cu concentration increases, indicating the strong possibility of direct electronic transitions.

The band gaps of these films are calculated using the following equation[8]:

$$\alpha h\upsilon = A(h\upsilon - Eg)^r, \tag{3}$$

where α is the coefficient of absorption, h is the Planck's constant, υ is the frequency of fallen light, Eg is the optical energy gap of the material, r is the factor controlling the direct and indirect translation of the electrons from the valence band to the conduction band, A is constant, and $h\nu$ is the energy of photon. Figure 9 shows the relationship between $(\alpha h\nu)^2$ and energy of photon $h\nu$. The results indicate that an increase in the Cu content from 0 wt.% to 6 wt.% leads to a decrease in the band gap from 3.87 eV to 3.57 eV, as shown in Fig. 10. This

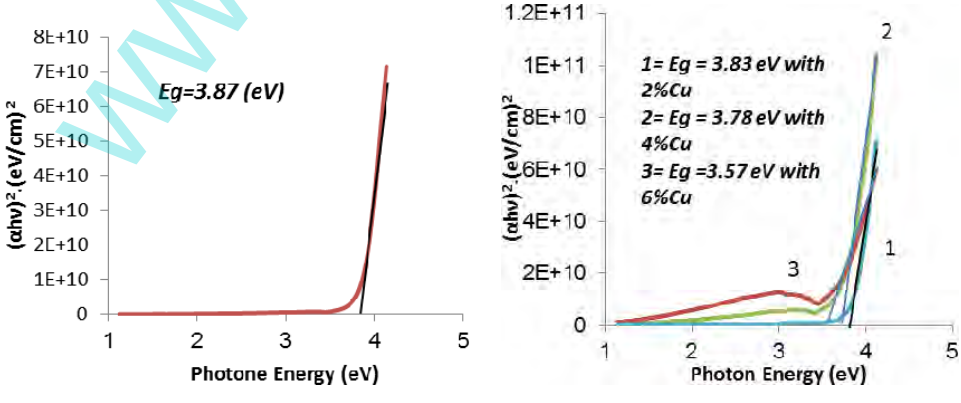

(a) (b)

Fig. 9. (Color online) $(\alpha h\nu)^2$ versus. Photon energy plot of (a) pure SnO_2 thin films (b) with different doping concentration of Cu.

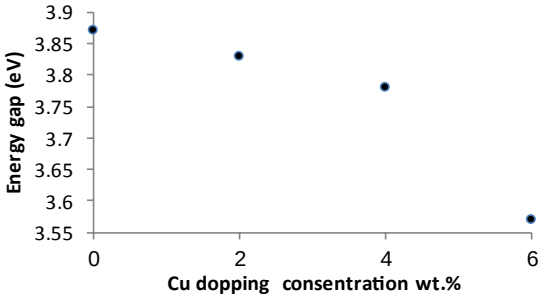

Fig. 10. (Color online) The energy gap as a function of doping concentrations of Cu doped SnO_2 thin films.

reduction in energy gap is caused by the presence of prohibited impurities that led to the formation of donor levels within the energy gap near the conduction band and these results are in agreement with those of Refs. 12 and 21.

Figure 11 shows the PL spectra of nondoped and Cu-doped SnO_2 (4 wt.% and 6 wt.% doping) obtained at room temperature. The spectrum displays two luminescence peaks; the first peak is positioned exactly at 320 nm UV emission and was caused by the near-band edge in the wide band gap of the SnO_2. The first peak was formed because of the recombination of free exciton through an exciton–exciton collision process.[23] The second peak positioned at 430–480 nm is the well-known blue emission band. Table 3 shows

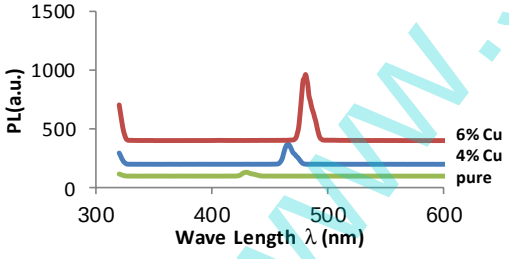

Fig. 11. (Color online) Photoluminescence spectra of pure and Cu- doped SnO_2 thin film.

Table 3. Energy values and intensity of PL peaks.

Cu-concentration	Wavelength of peak (nm)	Energy of peak (eV)
SnO_2 Pure	430	2.88
4% Cu	465	2.66
6% Cu	480	2.58

the peak energy values and the intensity of the luminescence spectrum of the samples. For the pure SnO_2 and all the doped films, a strong PL band with a peak position centered in 2.88 eV (430 nm) is obtained and this is less than that of the optical band gap of SnO_2 film 3.87 eV because of the oxygen vacancies that trap electrons from the surface, thereby causing this difference of the calculated energy gap from Tauc's law. This result agrees with that of Ref. 24. Therefore, the emission peak might correspond to the electron transition from the donor level formed by oxygen vacancy to the valance band in film. The electron in the donor level jumps to the valence band and the transition generates violet light emission, as shown in Fig. 11. XRD also shows the effect of doping on the crystallinity of SnO_2 thin film. The PL emission might be closely related to the luminescence of the recombination of photo-induced electrons and holes. The intensity of the light-emission peak increases initially as the doping concentration increases and reaches its maximum at 6 wt.% Cu-doping concentration. This is caused by the electron transition between 5d-excited state to 4f state that is located in the UV region.[25]

5. Electrical Conductivity

Electrical conductivity of SnO_2 thin films was measured at temperatures ranging from 303 K to 433 K. Electrical conductivity in all SnO_2 films increases exponentially as the temperature increases and this represents common semiconductor property, that is, the charge carrier concentration increases when the temperature increases. Figure 12 shows the relationship between $Ln\sigma$ and $1000/T$ for different Cu-doping concentrations. The activation energies E_{a1} and

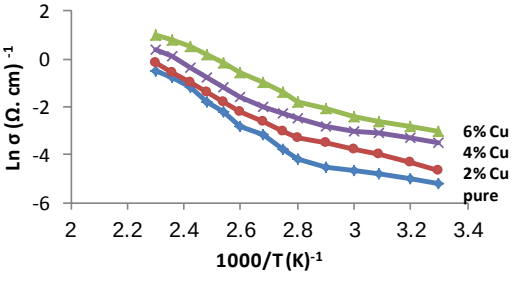

Fig. 12. (Color online) $Ln\sigma$ as a function of $1000/T(K)^{-1}$ for SnO_2 thin films for various doping concentrations with copper.

Table 4. Activation energies E_{a1} and E_{a2} for SnO_2 thin films for various doping concentrations with copper.

Cu-concentration	Activation energy E_{a1} (eV)	Activation energy E_{a2} (eV)
SnO_2 Pure	0.5	0.035
2% Cu	0.55	0.04
4% Cu	0.61	0.046
6% Cu	0.65	0.05

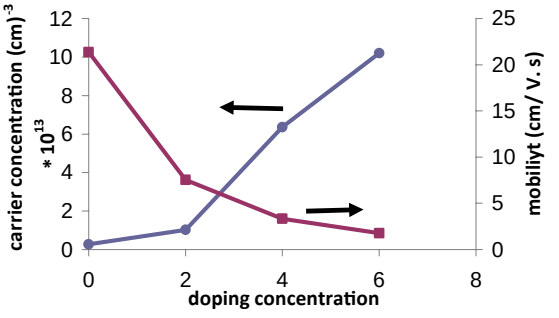

Fig. 13. (Color online) The carrier concentration and mobility of SnO_2 as a function of different doping concentrations with copper.

E_{a2} increase with increasing doping concentration in the films because of the donor formation by Oxygen vacancies and these results agree with that of Refs. 26 and 13. The energy activation is calculated using the formula[27]

$$\sigma = \sigma_o \exp(E_a/kT), \tag{4}$$

where σ is the conductivity at heat T, σ_o is constant, k is the Boltzmann constant, T is the temperature absolute, and E_a is the activation energy. Table 4 shows the activation energies E_{a1} and E_{a2} of the SnO_2 thin films for various doping concentration with Cu.

Hall measurements indicate that the SnO_2 thin films have good performance with n-type conductivity. As shown in Fig. 13 and Table 5, the value of electrical conductivity significantly increased along with an increase in the values of charge carriers as the values of both the mobility and Hall coefficient decreased. The concentration variation of the carrier can be ascribed to the substitution of Cu for oxygen, resulting in generation of conduction electrons that leads to the increase of carrier concentration. In different doping levels, the substitution of Cu for oxygen is the main defect in SnO_2:Cu films. In the substituent, each Cu^{+2} substitutes an O^{-2} in the lattice and the substituted O^{-2} provides more free electrons, which actively affects the free carrier initially. The mobility of SnO_2:Cu films continuously decreases with increasing Cu concentration. The actual value of mobility is dependent on the interaction between the various scattering centers and free carriers. These results are in good agreement with that obtained by Refs. 28 and 29.

6. Sensing Properties

The sensitivity (S) of SnO_2 gas sensor is typically defined as the rate of the surface resistance R_a of the film in air to that in the target gas R_g,[30] i.e.

$$S = \left| \frac{Rg - R_a}{R_a} \right| \times 100. \tag{5}$$

Figure 14 shows the sensitivity of pure and Cu-doped SnO_2 on glass substrate in different concentrations under the following conditions: increasing time at room temperature, 50°C operating temperature and CO concentration at approximately 50 ppm. The sensitivity of all samples, including sensitivity to CO, is increasing linearly with Cu-doping concentration. The sensitivity of pure SnO_2 is less than that of doped SnO_2. SnO_2 doped with 6 wt.% Cu has maximum sensitivity at room temperature and 50°C and this enhanced sensitivity could be attributed to an

Table 5. The obtained results of Hall measurement for SnO_2 at different annealing temperatures and Cu-doping concentrations.

Deposition condition		$R_H(m^{2/C})$	μ_H ($cm^2/v \cdot s$)	n $(cm)^{-3}$	Electric conductivity $(\Omega \cdot cm)^{-1}$
Cu-doping concentration	Pure	2.366×10^6	21.35	0.2638×10^{13}	9×10^{-6}
	2%	6.113×10^5	7.531	1.021×10^{13}	1.2×10^{-5}
	4%	9.82×10^4	2.34	4.36×10^{13}	2.3×10^{-5}
	6%	6×10^4	1.77	10.2×10^{13}	2.9×10^{-5}

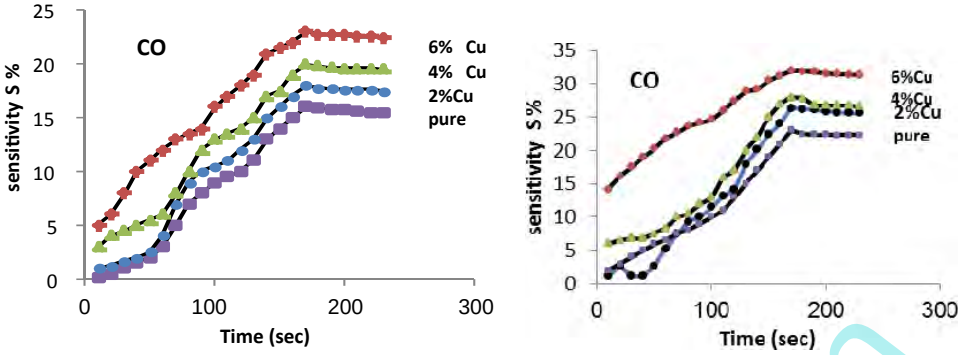

(a) (b)

Fig. 14. (Color online) The sensitivity S as a function of time plot of SnO_2 thin films for different doping concentrations of Cu (a) at room temperature, (b) at operating temperature, $T = 50°C$.

increased oxygen deficiency and/or to a positive catalytic effect caused by Cu-doping into SnO_2 and Cu-doping accelerates the adsorption/reaction of CO on the surface. Furthermore, the smaller grain size of the Cu-doped sensors compared with that of pure SnO_2 may also contribute to the improved sensor response.[31,32] The sensitivity of all samples is illustrated in Table 6.

Table 6. Values of sensitivity S % of pure SnO_2 and Cu dopant at room temperature and 50°C.

Cu-concentration	Sensitivity S% at 50°C	Sensitivity S % at room temperature
SnO_2 Pure	23	16
2% Cu	26.4	18
4% Cu	28	20
6% Cu	32	23

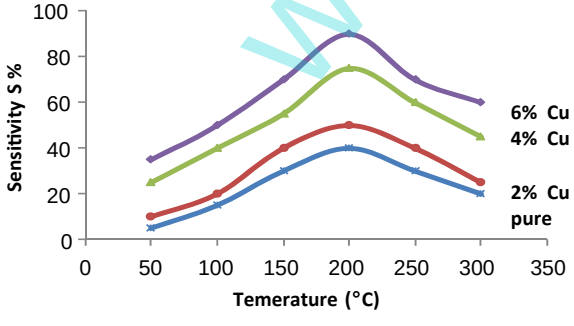

Fig. 15. (Color online) The sensitivity S% as a function of temperature plot of SnO_2 thin films for various doping concentrations of Cu for CO gas.

As shown in Fig. 15, the sensor sensitivity increases with increasing operating temperature and the optimal heat (200°C), which is the maximum peak values at certain temperatures, reduces with further increase in temperatures up to 300°C. The increase in density of charge carrier in the energetic surface results in a reduction in resistivity, thereby resulting in increased sensitivity as the operating temperature increases. Highest sensitivity appeared at 200°C and at temperatures higher than such, the sensitivity is reduced. This behavior may be attributed to the more frequent reaction of adsorbed oxygen species as the operating temperature increases, and more electrons, which are released because of this reaction, are sent back to conduction band, i.e. the desorption ratio of adsorbed gases also increases with increasing temperatures.[33] As the temperature further increases, more adsorbed oxygen species react and more electrons are sent back to conduction band, leading to increased conductivity. At 200°C, which is the critical temperature T_c, almost all adsorbed oxygen species react and electrons return to conduction band, leading to maximum sensitivity. The decrease in sensitivity to temperatures above the critical operating temperature, T_c, can be attributed to the higher desorption rates at these temperatures. When the target gases are introduced, the added desorption is caused by the target gases, which are comparatively small for the stable-state desorption in air, leading to reduced influence on the sensor response for $T > T_c$. Given the competition rates of adsorption and desorption, SnO_2 sensors always tend to display maximum sensitivity at a particular operating temperature.

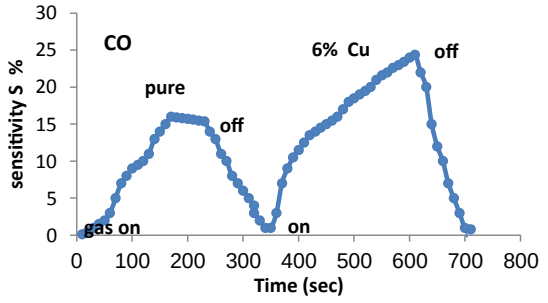

Fig. 16. (Color online) The response and recovery times for pure SnO_2 films and 6% Cu-doping for CO gas by dip-coating.

Table 7. The value of response and recovery times for pure SnO_2 films and Cu-doping at the exposition to CO gas.

Response time for pure	Recovery time for pure	Response time for 6% Cu	Recovery time for 6% Cu
80 s	100 s	140 s	80 s

Figure 16 hows the response and recovery times for pure SnO_2 thin films and 6 wt.% Cu-doping upon exposure to CO at 50 ppm concentration. Pure thin films derived through dip-coating have significantly faster response and recovery time compared with that of thin films derived through 6 wt.% Cu-doping, whereas Cu-doped films have higher sensitivity compared with pure films. The response and recovery times of pure SnO_2 and SnO_2 doped with 6 wt.% Cu thin film to CO at room temperature is illustrated in Table 7.

7. Conclusion

Pure and Cu-doped SnO_2 thin films were deposited on clean glass substrates through dip-coating sol–gel method. The deposited film was 300 nm thick, and XRD studies of as-deposited samples show polycrystalline structure with clear characteristic peak of the tetragonal rutile structure of SnO_2 with highly (110) preferred orientation. With Cu-doping from 0 wt.% to 6 wt.%, the prepared film has a good transmittance of 82.4–65.3% in the visible region and energy band gap of approximately 3.87–3.57 eV. The average optical transparency in the visible region and the direct optical band gap of thin films reduce with increasing Cu-doping concentration. The sensitivity of all samples, including CO, was noted to increase with Cu-doping and doping with 6 wt.% Cu results in maximum sensitivity of 23 at room temperature and 32 at 50°C. Based on the analysis of Cu-doped SnO_2 thin films, the thin film doped with Cu at 6 wt.% had high sensitivity for carbon monoxide gas at room temperature and 50°C. This means that Cu-doping at 6 wt.% significantly improves the performance and capability of SnO_2 thin films as gas sensors.

References

1. G. Sberveglieri, *Sens. Actuators* **23** (1995) 103.
2. W. Göpel and K. D. Schierbaum, *Sens. Actuators* **26** (1995) 1.
3. R. A. Rani, A. S. Zoolfakar, A. P. O'Mullane, M. W. Austin and K. Kalantar-Zadeh, *J. Mater. Chem.*, **2** (2014) 15683.
4. H. Rena, H. Huoa, P. Wangb, C. Wanga, S. Liub, M. Shena, H. Sunb and M. Ruthsc, *Int. J. Smart Nano Mater.* **5** (2015) 257.
5. D. P. Hermida, Y. R. Tayubi and R. Nopriyanti, *Int. J. Eng. Technol.* **13** (2013) 70.
6. S. J. Ikhmayies and R. N. Ahmad-Bitar, *Appl. Surf. Sci.* **255** (2008) 2627.
7. K. A. Mishjil, S. S. Chiad, H. L. Mansour and N. F. Habub, *J. Electron Dev.* **14** (2012) 1170.
8. C. H. Liu, L. Zhang and Y. Jin He, *Thin Solid Film*, **304** (1997) 13.
9. Yanxue Chen and Jun Jiao, *Int. J. Mod. Phys.* **23** (2009) 1904.
10. L. M. Dler, T. Sahm, A. Gurlo, J. D. Grunwaldt and N. Barsan, *J. Nanoparticle Res.* **8** (2006) 783.
11. J. Joseph, V. Mathew, J. Mathew and K. E. Abraham, *Turk. J. Phys.* **33** (2009) 37.
12. E. W. Williams, N. Tomlinson, M. T. Cheney and A. G. Keeling, *J. Mater. Sci., Mater. Electron.* **11** (2000) 369.
13. M. Parthibavarman, V. Hariharan, C. Sekar and V. N. Singh, *J. Optoelectron. Adv. Mater.* **12** (2010) 1894.
14. R. A. Ismail, S. M. H. Al-Jawad and N. Hussein, *Appl. Phys. A* **117** (2014) 1977.
15. X. Hong-Yan1, C. De-Liang and C. Bing-Qiang, Effect of nanoparticle size on gas-sensing properties of tin dioxide sensors, *Chem. Res. Chinese Universities* **28** (2012) 1086.
16. L. Mei and Y. Chen, *Sci. Rep.* **4** (2014).
17. Imad H. Kadhim and H. Abu Hassan, *J. Appl. Sci. Agri.* **10** (2015) 159.
18. F. E. Ghodsi and H. Absalan, *Acta Phys. Pol.* **118** (2010) 659.
19. P. Sagar, M. Kumar and R. M. Mehra, *Mater. Sci. Pol.* **23** (2005) 685.
20. M. R. Roknabadi, M. Behdani, H. Arabshahi and N. Hodeini, *Int. Rev. Phys.* **12** (2009) 153.

21. E. R. Leite, M. I. B. Bernardi, E. Longo, J. A. Varela and C. A. Paskocimas, *Thin Solid Films* **449** (2004) 67.
22. A. K. hudheir. S. S. Chiad, H. L. Mansour and N. F. Habub, *J. Electron Dev.* **14** (2012) 1170.
23. S. Ilican, Y. Caglar and M. Caglar, *J. Optoelectron. Adv. Mater.* **10** (2008) 2578.
24. Y. Zhu and X. Zhang, *Eur. J. Chem.* **2** (2011) 8.
25. S. Chen and X. Zhao, *Appl. Surf. Sci.* **258** (2012) 3255.
26. B. Zhang and Y. Tian, *J. Mater. Sci.* **46** (2011) 1884.
27. R. D. Sakhare, G. D. Khuspe, S. T. Navale, R. N. Mulik, M. A. Chougule, R. C. Pawar, C. S. Lee, S. Sen and V. B. Pati, *J. Alloys Compnd.* **563** (2013) 300.
28. M. E. M. Hassouna, A. M. El-Sayed, F. M. Ismail, M. H. Khder, A. A. Farghali and S. M. Yakout, *Int. J. Nanomater. Biostruct.* **2** (2012) 44.
29. B. Zhang and Y. Tian, *Mater. Lett.* **65** (2011) 1204.
30. S. K. Tripathy and B. P. Hota, *Afr. Rev. Phys.* **7** (2012) 401.
31. R. Savu, M. Adlfo and E. Joanni, *Mater. Res.* **12** (2009) 83
32. T. M. Hammad and N. K. Hejazy, *Int. Nano Lett.* **2** (2012) 2.
33. S. K. Tripathy and B. P. Hota, *J. Nano Electron. Phys.* **5** (2013) 04055.